The influence of land surface conditions and airmass history on extreme heat in the Central United States

Ronak N. Patel[1], Tapio Schneider[1], Sandra E. Yuter[2]

[1]Department of Environmental Science and Engineering, California Institute of Technology, Pasadena, CA, USA
[2]Department of Marine, Earth, and Atmospheric Sciences, North Carolina State University, Raleigh, NC, USA

Key Points:

- In the Southern Great Plains, extreme heat is amplified by sustained exposure of air parcels to dry soils along their upwind trajectories
- Hot-day trajectories (>95th percentile) arrive in southern Kansas with a potential temperature ~7K warmer than typical summer trajectories
- Decomposition of a mixed-layer budget attributes roughly 70–80% of the excess warming to reduced evaporative cooling from dry soils

Corresponding author: Ronak Patel, `ronak@caltech.edu`

Abstract

In the Central United States, extreme heat frequently co-occurs with soil moisture deficits and atmospheric aridity, amplifying agricultural impacts. Recent studies highlight the importance of viewing extreme heat as the integrated result of processes acting along air parcel trajectories rather than solely as a local phenomenon. Here, we investigate how upstream land surface conditions influence extreme summer temperatures in Kansas by computing 48-hour Lagrangian back trajectories in the boundary layer using HYSPLIT. ERA5 reanalysis from 1980–2022 is used to define hot summer days ($\geq$95th percentile) and typical summer conditions (47th–52nd percentile). We use a simplified mixed layer model to estimate the roles of surface heating (sensible and latent heat fluxes), entrainment, and radiative cooling on potential temperature along parcel pathways on hot and typical summer days. Hot day trajectories arrive in Kansas $\sim$7 K warmer than typical day trajectories. Along hot day trajectories, a larger surface heat flux from drier soils (reduced soil moisture evaporation) is the dominant contributor to the cumulative warming, exceeding the contribution from insolation by roughly a factor of three. Modest shifts in trajectory pathways expose air parcels to substantially drier upstream land surface conditions, leading to enhanced downstream warming. This Lagrangian perspective shows the importance of air-mass history in modulating regional heat extremes and has implications for the predictability of extreme heat in coupled land-atmosphere systems.

Plain Language Summary

Summer heat waves in the Central United States are often accompanied by dry soils, but it is unclear whether extreme temperatures are caused primarily by local land conditions or by air masses arriving from elsewhere. In this study, we combine atmospheric reanalysis data, soil moisture observations, and air parcel trajectory modeling to examine how heat builds along the pathways of air moving into the Southern Great Plains. We show that air masses associated with hot days tend to travel over drier regions of Texas and Oklahoma before reaching Kansas. As these air parcels move across dry soils, more surface energy is converted into sensible heating rather than evaporation, progressively warming the lower atmosphere. Using a simplified energy budget in the planetary boundary layer, we estimate that about 70–80% of the additional warming on hot days is associated with reduced evaporative cooling from dry soils. These results highlight the importance of upstream land surface conditions and atmospheric transport in shaping regional heat extremes.

1 Introduction

Summertime extreme heat poses cascading risks to human health (e.g., Robine et al., 2007; Matthews et al., 2025), energy infrastructure (e.g., Santamouris et al., 2015) and agricultural productivity (e.g., Schlenker & Roberts, 2009; Chen et al., 2021; Thornton et al., 2021; Abdelrahim & Jin, 2026). In the Central United States, extreme heat frequently co-occurs with soil moisture deficits, forming compound drought–heatwave events that amplify socioeconomic impacts (Zscheischler et al., 2020). In this part of the country, agricultural losses during hot summers are often more strongly driven by atmospheric aridity and extreme heat than by precipitation deficits alone (Rigden et al., 2020). Understanding the physical processes that intensify these temperature extremes is therefore critical for regional climate resilience in this agriculturally vital region where billions of dollars worth of corn, soybeans, and sorghum are grown in the summer.

Previous research using comprehensive earth system models has identified the US Southern Great Plains, northern India, East Asia, and the Sahel as key regions with strong soil moisture–temperature coupling, supported by both modeling (Koster et al., 2006; Seneviratne et al., 2010) and observational studies (Teuling et al., 2009; Gerken et al., 2019). In these regions, surface temperature variability is strongly constrained by the partitioning of available energy into latent and sensible heat fluxes. When soil moisture is abundant, more of the solar radiation is dissipated through evapotranspiration (latent heat fluxes), and the amount of evaporation is only limited by how much energy hits the ground. However, as soil moisture falls below a critical threshold and enters a soil moisture-limited regime, evaporative fraction decreases, sensible heat flux increases, and soil moisture becomes a first-order control on surface energy partitioning (Seneviratne et al., 2010; Duan et al., 2023). This transition enhances near-surface warming and can promote boundary layer growth and entrainment from the free troposphere, reinforcing land–atmosphere feedbacks that further dry the soil (Seneviratne et al., 2010; Santanello et al., 2018). As soil moisture decreases below the wilting point, soil water becomes increasingly unavailable for evapotranspiration because it is held tightly by the soil matrix (Seneviratne et al., 2010). The sensitivity of surface fluxes to soil moisture is maximized in transitional regimes between wet and dry climates, where evapotranspiration responds strongly to soil moisture variability, and is weaker in persistently wet or arid regions (Koster et al., 2004; Guo et al., 2006; Seneviratne et al., 2010). The impact of soil moisture on latent and sensible heat fluxes therefore matters most when the soil moisture is in the transitional zone where an increase in soil moisture is approximately linearly related to an increase in latent heat flux (Seneviratne et al., 2010; Duan et al., 2023).

While the relationship between local soil moisture deficits and extreme heat is well-established (e.g., Mueller & Seneviratne, 2012; Huybers et al., 2014; Miralles et al., 2018), local coupling alone often does not fully explain the magnitude and rapid intensification of large scale extreme heat. Increasing evidence suggests that non-local processes, particularly horizontal advection of heat from upstream regions, play a critical role. For example, by examining both local and upstream conditions during the 2010 Russian heatwave, Miralles et al. (2014) estimated that up to 40% of the heat stored in the atmospheric boundary layer was supplied by large-scale horizontal advection from regions with drier soils, with additional work demonstrating the combined importance of circulation and land surface conditions (Schumacher et al., 2019). Similarly, Lagrangian analyses of Australian heatwaves show that air parcels can warm by almost 10 K as they traverse regions of anomalous sensible heat flux before reaching the target region (Quinting & Reeder, 2017). These studies highlight the importance of viewing extreme heat as the integrated result of processes acting along air parcel trajectories rather than solely as a local phenomenon.

Despite this evidence, the role of non-local land–atmosphere interactions remains less well understood in the Central United States, particularly for more frequent (e.g., 95th percentile) heat extremes rather than rare, record-breaking events. This region is dynamically active and strongly influenced by the Great Plains Low-Level Jet (GPLLJ), which facilitates rapid poleward transport of air masses across the Southern Great Plains (Weaver & Nigam, 2008). As a result, upstream land surface conditions may exert a strong influence on downstream temperatures by preconditioning air masses prior to arrival. However, disentangling the roles of atmospheric circulation and upstream land surface conditions remains challenging using traditional Eulerian approaches.

To address this, we adopt a Lagrangian framework to characterize the thermodynamic and land surface history of air masses arriving in the Central U.S. near Wichita, Kansas during extreme summertime heat events. Using ERA5 reanalysis, GLEAM soil moisture data, and backward trajectories from HYSPLIT forced with HRRR meteorology, we track the evolution of key atmospheric variables along air parcel pathways and compare hot days to typical summer conditions. This approach allows us to explicitly link upstream land surface conditions to downstream temperature extremes.

We show that extreme heat in the Southern Great Plains emerges from multi-day preconditioning of air masses as they traverse regions of anomalously low soil moisture. In particular, trajectories associated with hot days preferentially pass over climatologically drier regions of central and western Texas, where enhanced sensible heat flux leads to progressive warming of the boundary layer prior to arrival. These results suggest that while local soil moisture deficits contribute to extreme heat, the pathways taken by boundary layer air across spatial gradients in land surface conditions play a large role in amplifying temperature extremes.

These findings have important implications for understanding and predicting extreme heat. Because temperature extremes depend not only on local conditions but also on upstream land surface states and atmospheric transport pathways, accurate prediction may require accounting for the spatial structure of soil moisture and its interaction with spatiotemporal variations in low-level winds. More broadly, this work highlights the importance of viewing extreme heat as a spatially integrated process shaped by both land surface heterogeneity and atmospheric dynamics.

2 Data and Methods

We use different datasets to define the large-scale atmospheric conditions associated with extreme heat, the corresponding land conditions, and high resolution data used in the trajectory analysis. ERA5 reanalysis (Hersbach et al., 2020) is used to define >95th percentile extreme heat and provide large-scale weather variables. The Global Land Evaporation Amsterdam Model (GLEAM; version 3.8a) dataset (Martens et al., 2017) is used to provide the accompanying local soil moisture on those days. Finally, the NOAA High Resolution Rapid Refresh (HRRR; Dowell et al. (2022)) model, is used to force trajectories for analysis and obtain key variables along the trajectories.

2.1 Land Surface and Atmospheric Datasets

Atmospheric data are obtained from the European Center for Medium-Range Weather Forecasts (ECMWF) ERA5 reanalysis (Hersbach et al., 2020). We use daily mean 2-m air temperature, 2-m relative humidity, 10-m winds and mean sea level pressure (MSLP), computed from hourly data at $0.25° \times 0.25°$ spatial resolution, for the period 1980–2022. Surface soil moisture is taken from the Global Land Evaporation Amsterdam Model (GLEAM; version 3.8a) dataset, also at a $0.25° \times 0.25°$ spatial resolution (Martens et al., 2017). We use surface (0–10 cm) soil moisture as a proxy for moisture availability relevant to evapotranspiration and surface heat flux partitioning. GLEAM provides daily soil moisture estimates derived from satellite observations and reanalysis forcing, allowing spatially and temporally consistent coverage across the study domain. All analysis is restricted to the boreal summer months (June–August; JJA) over the continental United States.

At each grid point, we compute daily percentiles of temperature and soil moisture relative to the 1980–2022 JJA climatology based on the ERA5 and GLEAM data sets respectively. This percentile-based framework allows us to define and compare extreme conditions across regions with different mean climates and variability, effectively eliminating the effect of the marginal distributions (Bousquet & Bernardara, 2021). Hot days are defined as days where daily mean 2-m air temperature exceeds the 95th percentile at a given location. Typical summer days are those where the daily mean temperature falls between the 47th and 52nd percentiles.

2.2 HYSPLIT Backward Trajectories

To complement the Eulerian analysis of large-scale atmospheric and land conditions, we compute Lagrangian trajectories to analyze the airmass evolution as air parcels move towards south-central Kansas. To do this, we use the National Oceanic and Atmospheric Administration (NOAA) Air Resources Laboratory's (ARL) HYbrid Single-Particle Lagrangian Integrated Trajectory (HYSPLIT) model (Draxler & Rolph, 2010). In this model, advection and diffusion calculations are made in a Lagrangian framework following the transport of air parcels, allowing for the calculation of air parcel trajectories forced by a given atmospheric flow field. We force HYSPLIT with the 3 km × 3 km grid size, hourly NOAA High Resolution Rapid Refresh (HRRR; Dowell et al. (2022)) model. Since the HRRR model was not operational before the 2015 summer season, and no other model's meteorological forcings provided adequate coverage, resolution, and meteorological fidelity for our purpose, we restrict the trajectory analysis to 2015–2022. This yields 17 hot days. Since there are many more typical days in this time frame, we select the most recent 18 typical days for comparison. The full list of hot and typical days is provided in the Supporting Information.

For each event, HYSPLIT back trajectories are initialized at 0000 UTC on the following day, corresponding to one minute after the end of the selected day. We compute an ensemble of backward trajectories terminating near Wichita, Kansas (37.65°N, 97.43°W) at approximately 250 m above ground level. The 250 m level is chosen to represent near-surface boundary-layer air while avoiding surface-level numerical noise. The lowest model level is 8 m and vertical spacing is 15–30 m near the surface (Dowell et al., 2022). The ensemble of backward trajectories is initialized in the form of a 3 × 3 × 3 cube in the X, Y, and Z dimensions centered on the target latitude, longitude, and height. The offsets are ±1 grid point (∼3 km) in the horizontal and ±0.01 sigma units (∼100 m) in the vertical. This yields 27 backward trajectories for each day.

Trajectories are integrated 48 hours backward in time using HYSPLIT's handling of 3D advection using model vertical velocity. At each timestep, HYSPLIT outputs parcel latitude, longitude, and height above mean sea level. The HRRR meteorologicala files provide the associated terrain height, potential temperature, ambient temperature, rainfall, mixed layer depth, relative humidity, and downward solar flux. These values along the backward trajectories are used to interpret differences in thermodynamic evolution between hot and typical days identified in the Eulerian analysis.

2.3 Energy Budgets

From the HYSPLIT back trajectories, we estimate the temporal tendency of boundary layer potential temperature along parcel pathways using a bulk mixed-layer energy framework. We restrict the analysis to trajectories that remain below 2500m for the full 48-hour period prior to 00 UTC (n=259/459, 56% of hot day trajectories; n=308/486, or 63% of typical day trajectories). Given the observed soil moisture below each of parcels and assuming a wilting point SM_{wilt} of 0.10 and field capacity SM_{fc} of 0.45 (Xu et al., 2025), we can write an estimated total tendency of the air parcels. Thus, the total potential temperature tendency in the boundary layer following the flow (material derivative) is written as the sum of contributions from surface sensible heat flux, entrainment from above the boundary layer, and radiative cooling:

$$\frac{\mathrm{d}\theta}{\mathrm{d}t} \approx \left(\frac{\mathrm{d}\theta}{\mathrm{d}t}\right)_{\mathrm{surface}} + \left(\frac{\mathrm{d}\theta}{\mathrm{d}t}\right)_{\mathrm{entrainment}} + \left(\frac{\mathrm{d}\theta}{\mathrm{d}t}\right)_{\mathrm{rad.\ cooling}} \tag{1}$$

Surface sensible heat flux is estimated from available energy and evaporative partitioning:

$$\mathrm{SHF} = (1 - \mathrm{EF})\mathrm{AE} \tag{2}$$

where available energy AE equals $(R_n - G)$, where R_n is net shortwave radiation at the ground assuming a surface albedo of 0.2 (Duchon & Hamm, 2006), such that net radiation is approximated as 80% of incoming shortwave radiation. G is ground heat flux, prescribed as 40% of R_n for the first hour after sunrise (from 11–12 UTC in Wichita, KS), 10% of R_n for the next three hours (12–15 UTC), and zero for the following hours, falling in the range suggested by Stull (1988). This simple diurnal prescription captures the typical rapid morning decay of ground heat flux relative to net radiation. The evaporative fraction is parameterized as a function of soil moisture

$$\mathrm{EF} = \frac{\mathrm{SM} - \mathrm{SM}_{\mathrm{wilt}}}{\mathrm{SM}_{\mathrm{fc}} - \mathrm{SM}_{\mathrm{wilt}}} \tag{3}$$

bounded between 0.05 and 0.95. This formulation captures first-order soil moisture control on surface flux partitioning. Sensitivity tests indicate that results are not qualitatively sensitive to reasonable variations in wilting point and field capacity. Thus, the contribution of surface heating to boundary layer temperature tendency is then

$$\left(\frac{\mathrm{d}\theta}{\mathrm{d}t}\right)_{\mathrm{surface}} = \frac{\mathrm{SHF}}{\rho c_p h} \tag{4}$$

where ρ is air density, c_p is the specific heat of dry air, and h is boundary layer depth. Surface heating is only applied when the boundary layer is > 500m deep.

Warming due to the entrainment of free-tropospheric air into the mixed layer is parameterized following the zero-order mixed layer framework (Tennekes, 1973; Stull, 1988), which yields an entrainment warming tendency of

$$\left(\frac{\mathrm{d}\theta}{\mathrm{d}t}\right)_{\mathrm{entrainment}} = \frac{w_e \Delta\theta}{h} \tag{5}$$

This term is applied only when the boundary layer is sufficiently deep ($h > 500\,\mathrm{m}$) and the parcel resides within the mixed layer. The entrainment velocity w_e is diagnosed from the HYSPLIT/HRRR estimated rate of boundary-layer deepening, $w_e = \max(dh/dt, 0)$. This equates the deepening rate following the parcel with the entrainment velocity, and so folds any deepening due to advection across spatial gradients in boundary-layer depth into the entrainment term. The potential temperature jump across the capping inversion is held fixed at $\Delta\theta = 2\,\mathrm{K}$, although in reality it varies over the diurnal cycle and from day to day. Because entrainment is a secondary contributor to the budget (Figure 6c–d), the leading-order results are insensitive to reasonable variations in this value.

Radiative cooling is represented as a constant longwave cooling tendency of

$$\left(\frac{\mathrm{d}\theta}{\mathrm{d}t}\right)_{\mathrm{rad.\ cooling}} = -0.2\ \mathrm{K\,hr^{-1}} \tag{6}$$

chosen to approximate typical clear-sky cooling rates in summertime continental boundary layers (Stull, 1988).

Observed tendencies are computed directly from trajectory data as finite differences in potential temperature over time. All budget terms are computed at each hour when trajectory information is saved from HYSPLIT and is subsequently composited across events using the mean.

To attribute differences in boundary layer potential temperature tendencies between hot and typical days, we decompose the surface-driven heating term in Equation (4) into contributions from soil moisture and insolation differences. We decompose differences between hot and typical conditions by expressing each variable as the sum of a reference (typical-day) value and a perturbation (hot-minus-typical anomaly), e.g., $\mathrm{AE} = \mathrm{AE}_{\mathrm{ref}} + \Delta\mathrm{AE}$, where reference values are defined as the mean diurnal evolution of typical days.

$$\Delta\left(\frac{d\theta}{dt}\right)_{\mathrm{surface}} \approx \frac{1}{\rho c_p}\left(-\frac{AE_{\mathrm{ref}}}{h_{\mathrm{ref}}}\,\Delta EF + \frac{1 - EF_{\mathrm{ref}}}{h_{\mathrm{ref}}}\,\Delta AE\right) \tag{7}$$

The first-order Taylor series expansion above allows us to decompose contributions to the difference in potential temperature tendency between hot and typical days to contributions from soil moisture–controlled partitioning of surface fluxes (“surface flux partitioning effect”) and (ii) changes in available energy (“insolation effect”). We choose not

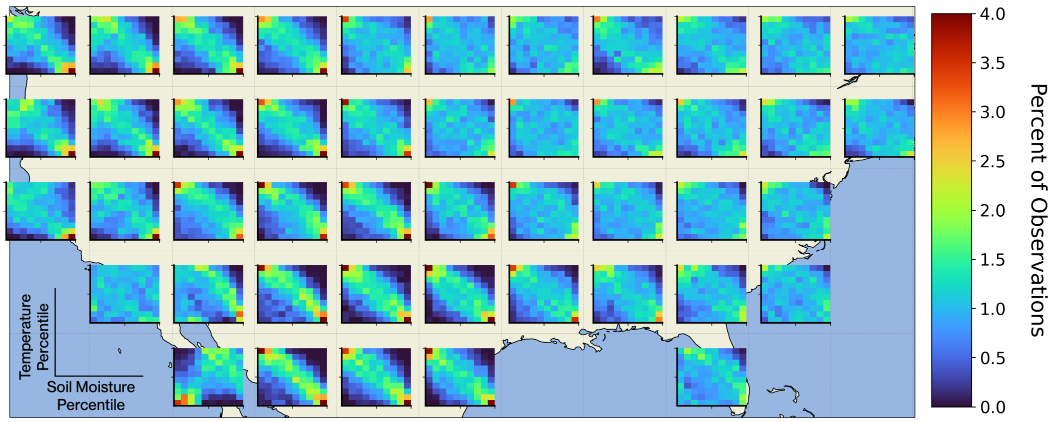

Figure 1. Joint 2D histograms of soil moisture percentile and temperature based on ERA5 during June, July, and August. Soil moisture percentiles are on the x-axis and temperature percentiles are on the y-axis with shading in the 2D phase space indicating the frequency of observations lying in each joint percentile bin. There are 10 soil moisture and temperature percentile bins. Therefore, 10% of observations occur in each row and column. Joint distributions and percentiles are calculated using the soil moisture and temperature time series averaged within each gridbox delineated by faint gray lines on the base map.

to estimate interaction terms and effects of changing boundary layer depth, which are secondary to available energy and the partitioning of surface heat fluxes. All terms are computed at each trajectory timestep and subsequently composited using the mean across events. Residual differences between the reconstructed and directly computed temperature tendencies are used to assess the validity of the decomposition.

3 Results

3.1 Large-Scale Atmospheric Patterns

We begin by using ERA5 atmosphere and GLEAM land reanalyses to examine the large-scale land-atmosphere patterns that produce extreme heat across the United States. We divide the continental United States into $5° \times 5°$ grid boxes. Within each grid box, we compute daily mean temperature and surface soil moisture for all summer days (JJA) from 1980–2022. For each grid box, we then construct a two-dimensional histogram of soil moisture percentile versus temperature percentile (Figure 1), where percentiles are defined relative to the local JJA climatology. The relationship between soil moisture and temperature varies substantially across regions in the United States. Across the Western US, we see the manifestation of a soil moisture-limited regime, where evapotranspiration is strongly controlled by soil moisture, leading to strong coupling between soil moisture and temperature through surface flux partitioning. In wetter regions across the Eastern US, evaporation is more energy limited, so the coupling between soil moisture and temperature is much weaker. In transitional regions between dry and wet climates, evapotranspiration exhibits strong sensitivity to soil moisture and there are large evapotranspiration variations (not shown), resulting in large variability in latent and sensible heat fluxes and enhanced land–atmosphere coupling.

The Southern Great Plains lies within this transitional regime of strong land–atmosphere coupling. We therefore focus on examining the characteristics of hot days in south-central

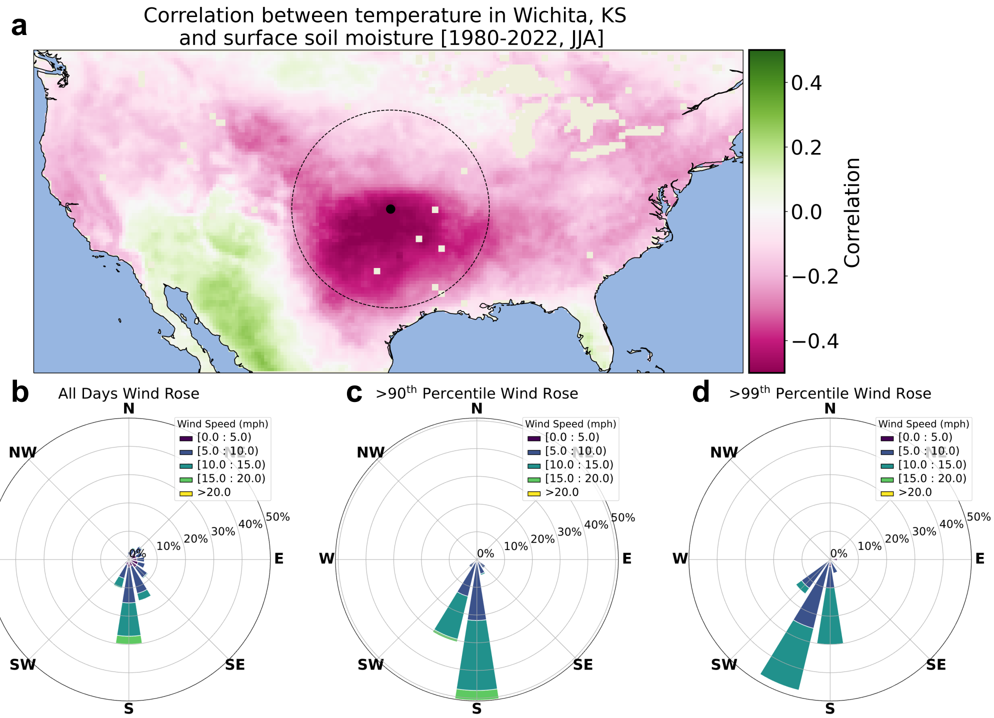

Figure 2. Overview of coincident local conditions of temperature and soil moisture across the continental US based on ERA5 (1980–2022) during June, July, and August. (a) A map of the Pearson correlation coefficient between the temperature in Wichita, KS and the surface soil moisture at each grid point. A circle centered on Wichita, KS with a radius equal to the e-folding distance of the temperature–soil moisture correlation is shown in dashed black. The location of Wichita is indicated by the black dot. (b) The wind rose for all summer days in Wichita, KS, where wind directions are divided into 16 directional bins, and the fraction of total observations in each bin dictate how long each sector is. Coloring is based on the wind speeds comprising each sector. (c) Same as (b) but for all days exceeding the summertime 90th percentile. (d) Same as (b) but for all days exceeding the summertime 99th percentile.

Kansas centered on Wichita. Across the summer season, temperature in Wichita, KS is negatively correlated with local soil moisture (r = –0.51), consistent with strong land–atmosphere coupling. Notably, temperature is also correlated with soil moisture located to the south of Wichita. This relationship extends over several hundred kilometers, with an e-folding length scale of approximately 850 km (Figure 2a), indicating a potential substantial influence of upwind land surface conditions. The e-folding distance is defined as the distance at which the correlation decreases to $1/e$ of its value in Wichita. This spatial structure is consistent with prevailing southerly winds in the region (Figure 2b), which transport air masses and their thermodynamic properties across the Southern Great Plains toward Kansas. On hot days where the temperature exceeds the 90th and 99th percentiles, we see a slight westerly component to the wind (Figure 2c–d). Although this shift is modest in magnitude, it plays an important role in modifying upstream source regions, as will be discussed later.

Focusing further on the large-scale land-atmosphere patterns giving rise to extreme heat in the Central US, we now look at composites of the temperature, soil moisture, and wind speed/direction on hot days in Wichita, KS and how they compare to typical days.

Conditioned on the daily mean 2m temperature exceeding the 95th percentile (31.0°C), the average temperature on all hot days is 31.7°C, which is 5.8°C above the summertime average. Temperatures exceed 30°C across most of the Southern Great Plains (Figure 3a) and temperature anomalies are greater than 5°C above typical days (Figure 3b), consistent with expectations of regionally coherent heat events. The local volumetric soil moisture is 0.25, which is 0.09 less than a typical day. On a larger-scale, we see lower soil moisture in western Texas, Oklahoma, and Kansas compared to the eastern portions of those states (Figure 3c) due to the climatologically drier soils in that area. Soil moisture anomalies of –0.05 to –0.10 are common in much of the Southern Great Plains (Figure 3d). Finally, we see that the winds on hot days, as with most days across this region characterized by the Great Plains Low Level Jet, are 4–5 m/s from the south (Figure 3e). On these hot days, there is an anomalous southwesterly component to the wind, and the winds are about 2–3 m/s faster. Also, the wind arrows in Figure 3f and MSLP anomalies (not shown) indicate the presence of a synoptic-scale low-pressure anomaly over eastern Nebraska. Overall, synoptic conditions associated with extreme heat are widespread soil moisture deficits co-occurring with elevated temperatures, and more locally, southwesterly winds ahead of a frontal boundary.

3.2 Trajectory Analysis

While the composite analysis highlights the large-scale co-occurrence of dry soils, anomalous winds, and extreme temperatures, it does not explicitly resolve the pathways through which land surface conditions influence downstream air masses. In particular, the spatial correlations and prevailing southerly flow suggest that the upwind land surface state may precondition air parcels prior to their arrival in southern Kansas. To directly examine this process, we adopt a Lagrangian framework and track the thermodynamic evolution of air parcels along their trajectories.

Figure 4 shows the ensemble of near-surface 48-hour backward trajectories that end near Wichita, KS on both hot and typical days from 2015 onward (see Methods), overlaid on the corresponding composite soil moisture fields. On typical days, the trajectories are more spatially dispersed and sample a wider range of upstream conditions, but generally come from the south and east. In contrast, on hot days, the trajectories exhibit a more spatially coherent plume passing west of the typical day plume, where soil moisture is climatologically lower.

To further investigate how these upstream conditions influence air parcel properties, we examine the temporal evolution of key thermodynamic and land surface variables along the trajectories. Figure 5 shows the evolution of air temperature, potential temperature, soil moisture, specific humidity, mixed layer depth, and incoming solar radiation along the 48-hour <2500m trajectory pathways (those trajectories that remain in/near the boundary layer for the entire period and are therefore influenced by surface conditions) for hot and typical days. Both air temperature and potential temperature are similar on hot days and typical days 48 hours before the arrival of the airmass in southern Kansas. Over the two day period, air temperature and potential temperature increase much more rapidly on hot days (Figure 5a–b). The soil moisture is lower over the entire path of parcel trajectories leading to hot days (Figure 5c). While there is a gradient in the median soil moisture across Texas (Figure 4), since parcels traverse this gradient at different times (typically 18–36 hours prior to arrival), the ensemble median reflects a gradual decline in soil moisture rather than a sharp transition. By around 6 hours prior to arrival in Wichita, the soil moisture on hot days is comparable to that on typical days. By this point, the parcel trajectories on hot and typical days are both passing over the wetter soils of Central Kansas. The specific humidity approximately 36–48 hours before hot and typical days are similar, but there is a rapid decrease the day before a hot day (Figure 5d), largely due to entrainment of dry free-tropospheric air (not shown). We also see that the mixed layer is deeper on hot days compared to days with

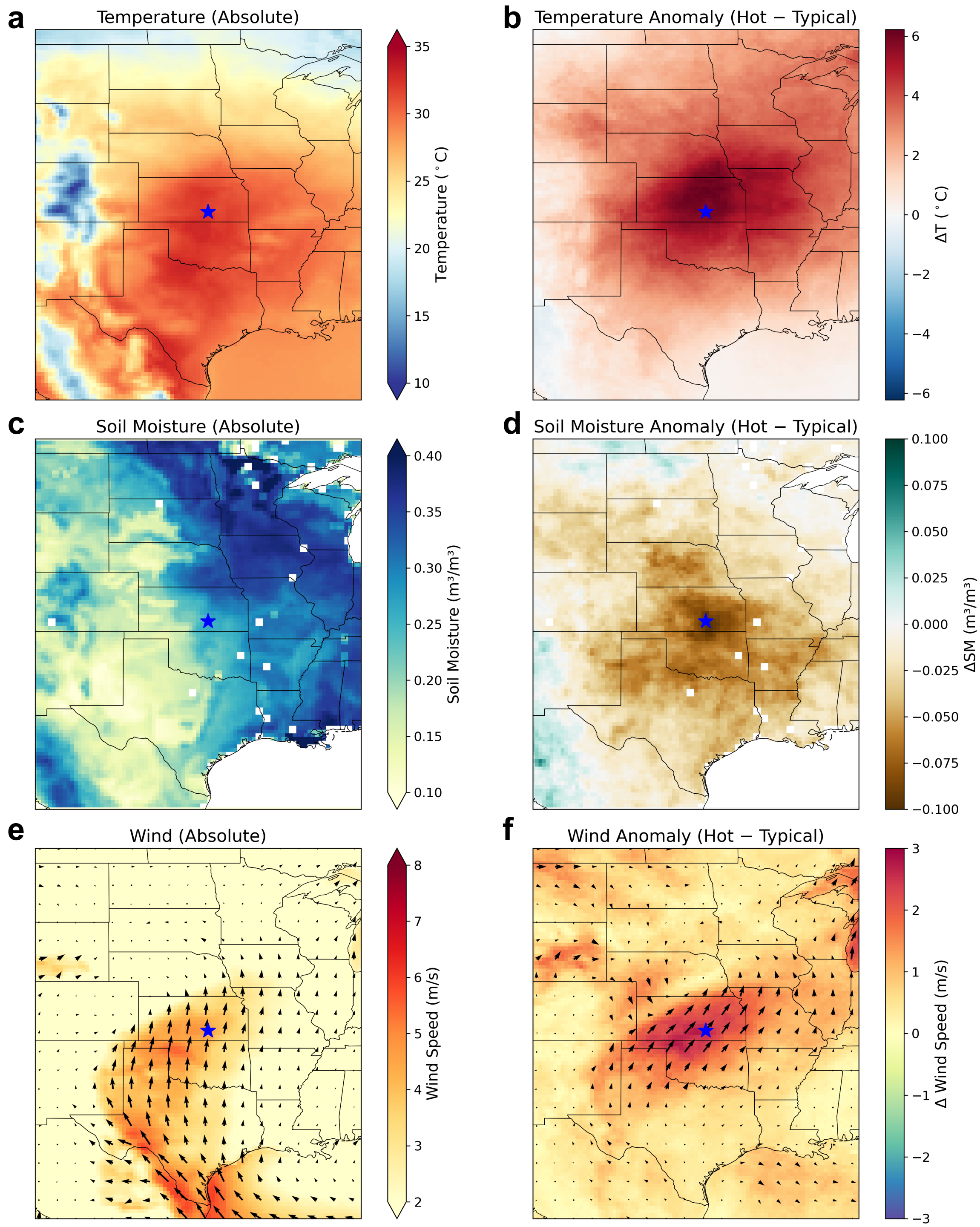

Figure 3. Multipanel plot showing composite maps of large-scale features of the days where the temperature is above the 95th percentile in Wichita, KS from 1980–2022 (n = 198 days) based on ERA5. (a) Map of temperature. (b) Map of the temperature anomaly as calculated by the difference between the mean temperature on hot days minus the mean temperature on the typical days (n=198). (c) Map of volumetric surface soil moisture. (d) Map of soil moisture anomaly. (e) Map of the mean wind speed shown by shading. Wind vectors are shown by the arrows overlaid on the plot. (f). Map of the wind speed anomaly shown by shading. Wind vector anomalies are indicated by arrows. Arrows in this panel with the same length as those in panel (e) are 0.5x as fast. The location of Wichita, KS is shown by a blue star on all subpanels.

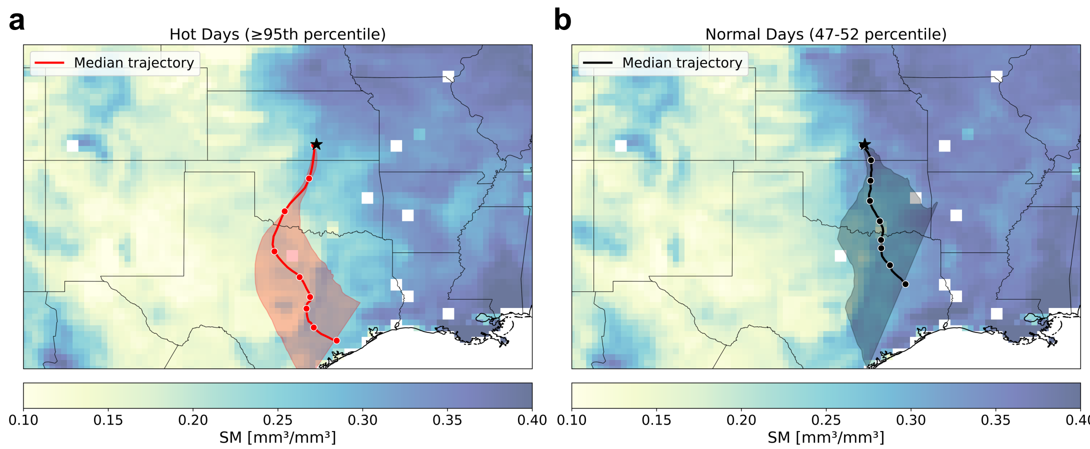

Figure 4. Plot of HYSPLIT back trajectories that occur entirely below 2500m on (a) the 17 hot days and (b) the 18 typical days with the interquartile range of trajectory positions at each time step shaded in each plume. The hourly median is shown by a solid line with circles plotted every six hours at 00, 06, 12, and 18 UTC. Hot day plumes are shown in red and typical day plumes are shown in black. Plumes are overlaid on the median volumetric soil moisture on the days where the trajectories occur.

a more typical temperature (Figure 5e). Finally, we see that hot days have slightly more insolation than typical days (Figure 5f), consistent with reduced cloud cover. Together, these results indicate that air parcels associated with hot days experience sustained exposure to drier land surfaces, deeper boundary layers, and enhanced radiative forcing, all of which contribute to amplified warming during transport.

These results raise a key question: what processes along the trajectory are responsible for the enhanced warming observed on hot days? In particular, the co-occurrence of reduced soil moisture and enhanced radiative forcing suggests that multiple mechanisms may contribute to the observed temperature differences. To quantify the relative contributions of these processes, we next evaluate a mixed-layer energy budget along the trajectories. This framework allows us directly attribute the cumulative warming along the trajectory to distinct physical processes.

3.3 Attribution of Extreme Heat on Hot Days

To quantify the physical drivers of excess warming along hot-day trajectories, we apply the bulk mixed-layer potential temperature budget (Methods) to each trajectory that remains below 2500 m throughout the 48-hour period. Surface, entrainment, and radiative cooling tendencies are computed hourly using HRRR meteorological fields and GLEAM soil moisture along HYSPLIT back trajectories. For hot-day trajectories, we further decompose anomalies in surface heating relative to a typical-day reference state into contributions from surface flux partitioning (evaporative fraction/soil moisture) and available energy using a first-order Taylor expansion.

To demonstrate that the simplified mixed-layer model is adequate for purpose (Parker, 2020), we compare the output of the mixed-layer model to reference values from HYSPLIT/HRRR. The simplified mixed-layer budget model qualitatively reproduces the HYSPLIT/HRRR mean diurnal cycle of potential temperature tendencies along both hot day and typical day trajectories (Figure 6a). Peak daytime heating rates are overestimated by approximately 0.2 K/hr for hot-day trajectories, while agreement is closer for typ-

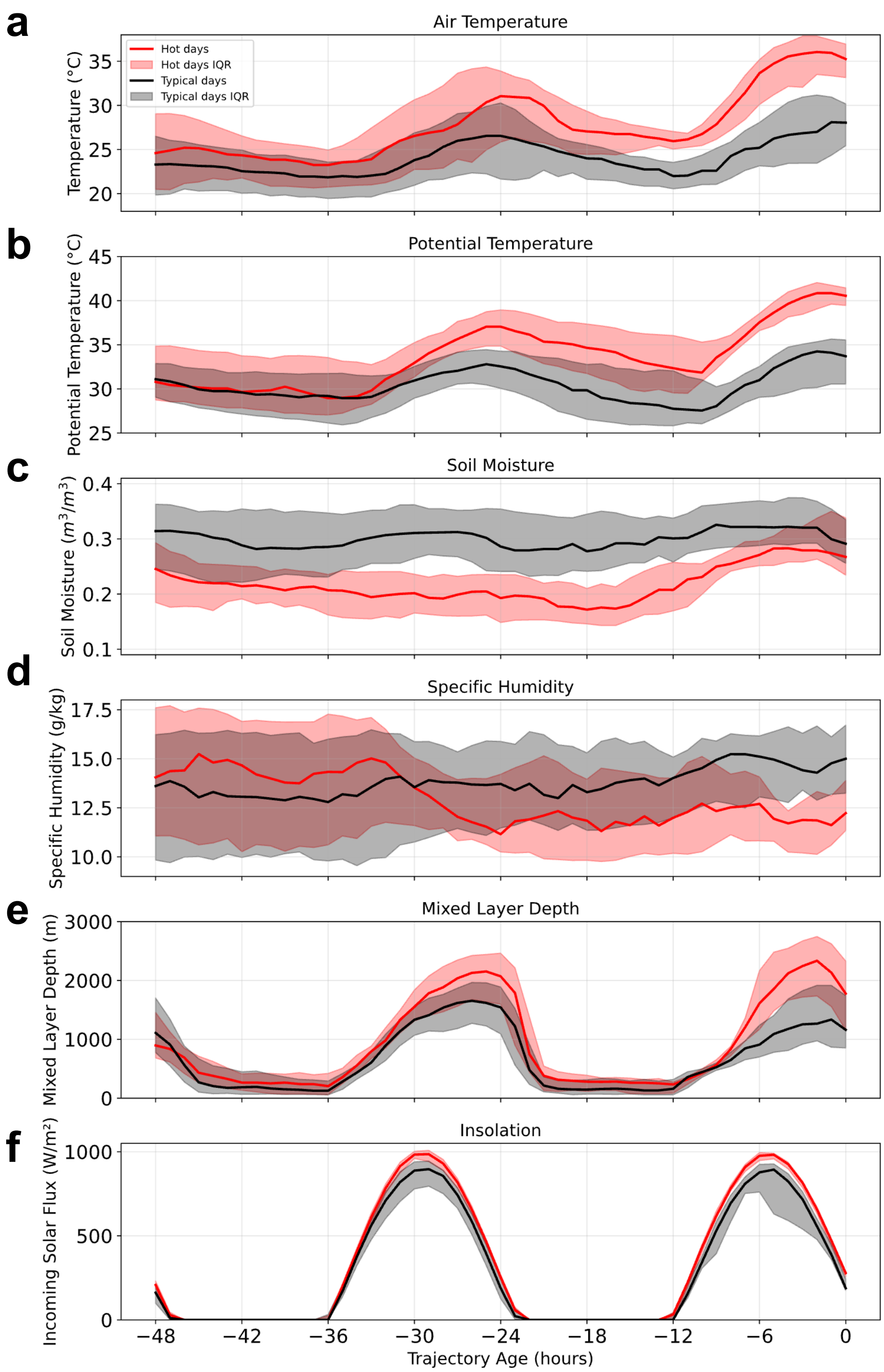

Figure 5. Time series evolution of (a) air temperature, (b) potential temperature, (c) soil moisture, (d) specific humidity, (e) mixed layer depth, and (f) incoming solar radiation from the HRRR model along the 48-hour HYSPLIT back trajectories that remain below 2500m (this is used as a proxy for boundary layer air) for their entire journey. Time is shown relative to arrival in Wichita ($t = 0$). The hourly median is shown by a solid line and the interquartile range is shaded. The time series for the hot days is in red and typical days are in black.

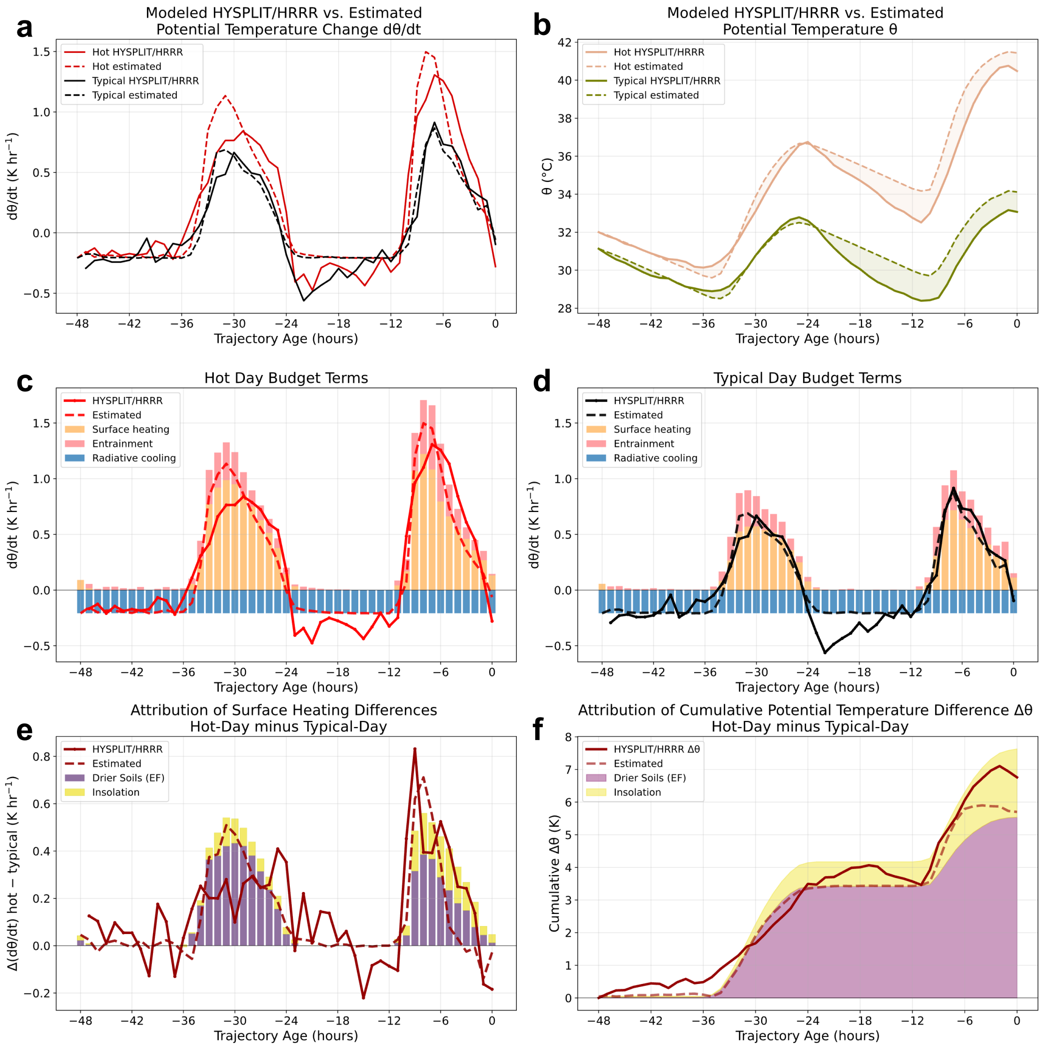

Figure 6. Comparisons between HYSPLIT/HRRR values (solid lines) and estimates from the simplified mixed-layer model (dashed lines) along 48-hour trajectories arriving at Wichita, KS (a–d). Stacked bars in (c–e) and shading in (f) indicate contributions of individual physical processes to the mixed-layer model based estimates. (a) Mean HYSPLIT/HRRR (solid) and model estimated (dashed) $d\theta/dt$ for hot (red) and typical (black) days. (b) Corresponding HYSPLIT/HRRR (solid) and reconstructed (dashed) θ, initialized from the earliest trajectory time and integrated forward using the estimated tendencies in (a), for hot days (dark beige) and typical days (green). (c–d) Decomposition of $d\theta/dt$ into surface heating (brown), entrainment (pink), and radiative cooling (blue) for (c) hot and (d) typical days; dashed lines show the sum of terms and solid black lines show HYSPLIT/HRRR tendencies. (e) Hot minus typical differences in the surface heating contribution to $d\theta/dt$ from panels c and d, separated into effects from drier soils/reduced evaporative cooling (purple) and increased available shortwave energy (yellow). The solid dark red line shows the observed HYSPLIT/HRRR mean difference and the dashed line shows the sum of all terms in the parameterized mixed layer model. (f) As in (e), but integrated in time to give cumulative θ differences.

ical days. Since the mixed-layer model only considers a constant longwave cooling rate, reflecting the simplified representation of nocturnal radiative cooling and the absence of stable boundary layer processes, there is some discrepancy in the cooling rate from –24 to –12 hours. Despite these and other limitations, the budget captures the key feature that hot-day trajectories experience systematically stronger daytime heating over multiple days prior to arrival. Integrating the estimated tendencies forward in time from the earliest trajectory age, when parcels are around 2000m above the surfaces, yields reconstructed potential temperature evolution that closely follows the values from HYSPLIT/HRRR (Figure 6b), with a cumulative warm bias of approximately 1 K at arrival, likely reflecting simplified nocturnal cooling and boundary layer dynamics.

Examining individual budget terms reveals how the balance of surface heating, entrainment, and radiative cooling differs on hot days compared to typical days (Figure 6c–d). On hot days (Figure 6c), surface sensible heat flux dominates the daytime heating tendency, with peak values around 1 K/hr, supplemented by a modest entrainment contribution during the morning boundary layer growth phase. On typical days, the same processes operate, but with substantially weaker surface heating (approximately 0.6–0.7 K/hr), reflecting wetter soils and reduced incoming shortwave energy (insolation) along the trajectories. The radiative cooling term, held constant at approximately -0.2 K/hr, provides the same cooling in both groups.

To isolate the drivers of the pronounced difference in surface heating between hot and typical days (the different height of the brown bars in Fig. 6c–d), we decompose the anomaly in surface heating (hot minus typical) at each time step using a first-order Taylor expansion (Figure 6e). For each trajectory, the surface heating anomaly is expressed as the sum of contributions from changes in soil moisture (via reduced soil moisture evaporation and thus less cooling) and insolation relative to a mean typical day reference state. These contributions are computed along each trajectory and then averaged across the ensemble of all trajectories. The results show that the reduced evaporative fraction due to drier soils accounts for the majority of the daytime heating anomaly, while increased incoming shortwave energy contributes a smaller but non-negligible component (Figure 6e). The sum of these terms (height of the bars) largely follows the HYSPLIT/HRRR tendency difference (solid line), indicating that these leading-order processes capture the dominant controls on enhanced warming (Figure 6e).

Integrating these contributions over the entire lifetime of the trajectory reveals their cumulative impact on the potential temperature difference at arrival (Figure 6f). Hot-day trajectories arrive approximately 7 K warmer than typical-day trajectories (the HYSPLIT/HRRR difference in Figure 6f), of which reduced evaporative fraction associated with drier soils accounts for approximately 70–80% (about 5 K), with increased insolation providing most of the remainder. The reconstructed difference closes about 5.5 K of the 7 K total, leaving a residual of order 1 K that is not attributed by the decomposition. This residual reflects differences in entrainment, neglected higher-order and boundary-layer-depth terms, and simplified nocturnal and stable-layer processes; it does not alter the leading-order balance, in which drier soils dominate.

Overall, these results demonstrate that land–atmosphere coupling through soil moisture depletion is the dominant driver of enhanced warming along hot-day trajectories. This effect is reinforced by increased insolation, but the primary control arises from the shift in surface flux partitioning toward sensible heating under dry soil conditions. Therefore, sustained exposure to dry soils along the trajectory plays a central role in amplifying downstream heat extremes.

4 Discussion and Summary

We have shown that extreme heat events in the Southern Great Plains arise from the combined effects of land–atmosphere coupling and synoptic-scale transport. Hot days are characterized not only by locally dry soils, but also by anomalous horizontal wind patterns that advect air parcels across systematically drier regions to the west and south. As a result, low-level air masses are progressively preconditioned through enhanced sensible heating prior to arrival, leading to amplified warming relative to typical days. This demonstrates that extreme heat in this region is not solely a local phenomenon, but instead reflects the integrated influence of upstream land surface conditions along the trajectory.

A key feature underlying this behavior is the strong east–west gradient in soil moisture across Texas and the Southern Great Plains, which closely aligns with the climatological transition zone where precipitation minus evaporation equals zero (the P–E=0 line as in Salley et al. (2016)). This gradient provides a spatially localized source of strong surface flux contrasts, such that relatively modest shifts in trajectory pathways can expose air parcels to substantially different land surface conditions. Variability in the position or intensity of this hydroclimatic transition may therefore play an important role in modulating extreme heat risk. In particular, years in which this transition zone shifts eastward may favor greater exposure of air parcels to dry soils, enhancing downstream warming.

The mixed-layer budget analysis further demonstrates that soil moisture–controlled surface fluxes are the dominant contributor to enhanced warming along hot-day trajectories, exceeding the contribution from increased insolation by roughly a factor of three (consistent with the 70–80% attribution above). While enhanced insolation consistent with reduced cloud cover (Domeisen et al., 2022) and even proximity to the solstice (Ndoping et al., 2026) contributes to warming, its effect is secondary to the reduced evaporative fraction due to drier soils, in agreement with previous results from an idealized surface energy balance model (Zeppetello et al., 2022). Together, these results indicate that sustained exposure to dry soils along the trajectory plays a central role in amplifying downstream temperature extremes.

These findings are consistent with previous studies highlighting the role of soil moisture–temperature coupling in amplifying record-breaking heat extremes (Miralles et al., 2014; Schumacher et al., 2019). Our results extend prior work by demonstrating that the impact of soil moisture is strongly mediated by atmospheric transport on hot days in the Southern Great Plains. Rather than reflecting purely local land–atmosphere feedbacks, extreme heat events emerge from the interaction between synoptic-scale circulation and spatial heterogeneity in land surface conditions. In particular, anomalous horizontal wind patterns equatorward of a cyclone to the north of Kansas modulate the upstream source regions traversed by air parcels, thereby controlling the degree of preconditioning prior to arrival. While the importance of upwind drought for record-breaking mega-heatwaves is established (Miralles et al., 2014; Schumacher et al., 2019), our results show that modest shifts in wind direction, by steering parcels onto the dry side of a sharp soil-moisture gradient, exert a comparable control on more frequent (95th-percentile) heat extremes in the Southern Great Plains.

The relatively short ($\sim$48-hour) timescale over which temperature differences emerge along trajectories suggests that extreme heat in this region is shaped by rapid preconditioning rather than long-term accumulation. This behavior is consistent with the presence of strong low-level winds associated with the Great Plains low-level jet, which limit the residence time of air parcels over any given surface region. As a result, the development of extreme heat depends on both the magnitude of land surface anomalies and the pathways through which air parcels are advected across them.

The bulk mixed-layer budget represents a simplified description of boundary layer processes, including entrainment parameterization, radiative cooling, local variations in soil characteristics, and surface heat flux partitioning. This analysis does not quantify the more uncertain processes of how boundary layer depth and entrainment from the previous day's residual layer contribute to extreme heat. While we assume that this effect is encompassed by the entrainment of free tropospheric air, a more realistic model would consider the evolving vertical profile of temperature above the boundary layer that would affect heating due to entrainment. The budget is also restricted to the 56% of hot-day and 63% of typical-day trajectories that remain below 2500 m for the full 48-hour period. Trajectories that rise out of the boundary layer are excluded and may sample different entrainment and mixing histories, so the composite reflects parcels that stay coupled to the surface. Despite these simplifications, the framework captures the leading-order differences between hot and typical days, suggesting that the primary driver is due to soil moisture effects.

These results have important implications for understanding and predicting extreme heat in regions characterized by strong land–atmosphere coupling. Because temperature extremes depend on both local conditions and upstream land surface states, accurate prediction may require accounting for the spatial distribution of soil moisture and its interaction with the low-level wind pattern. Furthermore, large-scale changes in soil moisture, land use, and circulation patterns under climate change and internal variability may alter the frequency and severity of extreme heat. While land surface processes are not the sole driver of extreme heat, this work shows the importance of viewing extreme heat as a spatially and temporally integrated process, shaped by both upstream land surface conditions and atmospheric dynamics.

Open Research Section

ECMWF ERA5 reanalysis data is available at Hersbach et al. (2023). GLEAM data is accessed at sftp://hydras.ugent.be and the required username and password are provided by GLEAM at https://www.gleam.eu/. HYSPLIT trajectories were obtained from https://www.ready.noaa.gov/hypub-bin/trajtype.pl?runtype=archive.

Conflict of Interest

The authors declare no conflicts of interest relevant to this study.

Acknowledgments

This research was supported by Schmidt Sciences, LLC. We also thank Kirsten Findell for helpful discussions and comments on this work. The authors also thank the NOAA Air Resources Laboratory (ARL) for the provision of the HYSPLIT transport and dispersion model and the READY website (https://www.ready.noaa.gov) used in this publication.

References

Abdelrahim, N. A. M., & Jin, S. (2026, February). Increasing compound drought and heatwave events in the horn of africa and its effect on agriculture. *Natural Hazards*, *122*(4). Retrieved from `http://dx.doi.org/10.1007/s11069-025-07850-8` doi: 10.1007/s11069-025-07850-8

Bousquet, N., & Bernardara, P. (Eds.). (2021). *Extreme value theory with applications to natural hazards: From statistical theory to industrial practice.* Springer International Publishing. Retrieved from `http://dx.doi.org/10.1007/978-3-030-74942-2` doi: 10.1007/978-3-030-74942-2

Chen, S., Yong, Y., & Ju, X. (2021, July). Effect of heat stress on growth and production performance of livestock and poultry: Mechanism to prevention. *Journal of Thermal Biology*, *99*, 103019. Retrieved from http://dx.doi.org/10.1016/j.jtherbio.2021.103019 doi: 10.1016/j.jtherbio.2021.103019

Domeisen, D. I. V., Eltahir, E. A. B., Fischer, E. M., Knutti, R., Perkins-Kirkpatrick, S. E., Schär, C., ... Wernli, H. (2022, December). Prediction and projection of heatwaves. *Nature Reviews Earth & Environment*, *4*(1), 36–50. Retrieved from http://dx.doi.org/10.1038/s43017-022-00371-z doi: 10.1038/s43017-022-00371-z

Dowell, D. C., Alexander, C. R., James, E. P., Weygandt, S. S., Benjamin, S. G., Manikin, G. S., ... Alcott, T. I. (2022, August). The high-resolution rapid refresh (hrrr): An hourly updating convection-allowing forecast model. part i: Motivation and system description. *Weather and Forecasting*, *37*(8), 1371–1395. Retrieved from http://dx.doi.org/10.1175/waf-d-21-0151.1 doi: 10.1175/waf-d-21-0151.1

Draxler, R., & Rolph, G. (2010). Hysplit (hybrid single-particle lagrangian integrated trajectory) model access via noaa arl ready website (http://ready. arl. noaa. gov/hysplit. php). noaa air resources laboratory. *Silver Spring, MD*, *25*(1).

Duan, S. Q., Findell, K. L., & Fueglistaler, S. A. (2023, April). Coherent mechanistic patterns of tropical land hydroclimate changes. *Geophysical Research Letters*, *50*(7). Retrieved from http://dx.doi.org/10.1029/2022GL102285 doi: 10.1029/2022gl102285

Duchon, C. E., & Hamm, K. G. (2006, January). Broadband albedo observations in the southern great plains. *Journal of Applied Meteorology and Climatology*, *45*(1), 210–235. Retrieved from http://dx.doi.org/10.1175/JAM2317.1 doi: 10.1175/jam2317.1

Gerken, T., Ruddell, B. L., Yu, R., Stoy, P. C., & Drewry, D. T. (2019, October). Robust observations of land-to-atmosphere feedbacks using the information flows of fluxnet. *npj Climate and Atmospheric Science*, *2*(1). Retrieved from http://dx.doi.org/10.1038/s41612-019-0094-4 doi: 10.1038/s41612-019-0094-4

Guo, Z., Dirmeyer, P. A., Koster, R. D., Sud, Y. C., Bonan, G., Oleson, K. W., ... Xue, Y. (2006, August). Glace: The global land–atmosphere coupling experiment. part ii: Analysis. *Journal of Hydrometeorology*, *7*(4), 611–625. Retrieved from http://dx.doi.org/10.1175/JHM511.1 doi: 10.1175/jhm511.1

Hersbach, H., Bell, B., Berrisford, P., Biavati, G., Horányi, A., Muñoz Sabater, J., ... Thépaut, J. (2023). *Era5 hourly data on single levels from 1940 to present. [dataset].* Copernicus Climate Change Service (C3S) Climate Data Store (CDS). doi: 10.24381/CDS.ADBB2D47

Hersbach, H., Bell, B., Berrisford, P., Hirahara, S., Horányi, A., Muñoz-Sabater, J., ... Thépaut, J. (2020, June). The era5 global reanalysis. *Quarterly Journal of the Royal Meteorological Society*, *146*(730), 1999–2049. Retrieved from http://dx.doi.org/10.1002/qj.3803 doi: 10.1002/qj.3803

Huybers, P., McKinnon, K. A., Rhines, A., & Tingley, M. (2014, September). U.s. daily temperatures: The meaning of extremes in the context of nonnormality. *Journal of Climate*, *27*(19), 7368–7384. Retrieved from http://dx.doi.org/10.1175/JCLI-D-14-00216.1 doi: 10.1175/jcli-d-14-00216.1

Koster, R. D., Dirmeyer, P. A., Guo, Z., Bonan, G., Chan, E., Cox, P., ... Yamada, T. (2004, August). Regions of strong coupling between soil moisture and precipitation. *Science*, *305*(5687), 1138–1140. Retrieved from http://dx.doi.org/10.1126/science.1100217 doi: 10.1126/science.1100217

Koster, R. D., Sud, Y. C., Guo, Z., Dirmeyer, P. A., Bonan, G., Oleson, K. W., ... Xue, Y. (2006, August). Glace: The global land–atmosphere coupling experiment. part i: Overview. *Journal of Hydrometeorology*, *7*(4), 590–610. Retrieved from http://dx.doi.org/10.1175/JHM510.1 doi: 10.1175/jhm510.1

Martens, B., Miralles, D. G., Lievens, H., van der Schalie, R., de Jeu, R. A. M., Fernández-Prieto, D., ... Verhoest, N. E. C. (2017, May). Gleam v3: satellite-based land evaporation and root-zone soil moisture. *Geoscientific Model Development*, *10*(5), 1903–1925. Retrieved from http://dx.doi.org/10.5194/gmd-10-1903-2017 doi: 10.5194/gmd-10-1903-2017

Matthews, T., Raymond, C., Foster, J., Baldwin, J. W., Ivanovich, C., Kong, Q., ... Horton, R. M. (2025, February). Mortality impacts of the most extreme heat events. *Nature Reviews Earth & Environment*, *6*(3), 193–210. Retrieved from http://dx.doi.org/10.1038/s43017-024-00635-w doi: 10.1038/s43017-024-00635-w

Miralles, D. G., Gentine, P., Seneviratne, S. I., & Teuling, A. J. (2018, June). Land–atmospheric feedbacks during droughts and heatwaves: state of the science and current challenges. *Annals of the New York Academy of Sciences*, *1436*(1), 19–35. Retrieved from http://dx.doi.org/10.1111/nyas.13912 doi: 10.1111/nyas.13912

Miralles, D. G., Teuling, A. J., van Heerwaarden, C. C., & Vilà-Guerau de Arellano, J. (2014, April). Mega-heatwave temperatures due to combined soil desiccation and atmospheric heat accumulation. *Nature Geoscience*, *7*(5), 345–349. Retrieved from http://dx.doi.org/10.1038/ngeo2141 doi: 10.1038/ngeo2141

Mueller, B., & Seneviratne, S. I. (2012, July). Hot days induced by precipitation deficits at the global scale. *Proceedings of the National Academy of Sciences*, *109*(31), 12398–12403. Retrieved from http://dx.doi.org/10.1073/pnas.1204330109 doi: 10.1073/pnas.1204330109

Ndoping, S., Robson, J., Mareshet Admasu, L., Chui, T. C. Y., Howard, R., & White, R. H. (2026, February). The role of near solstice solar radiation on the pacific northwest heatwave of june 2021. *Geophysical Research Letters*, *53*(3). Retrieved from http://dx.doi.org/10.1029/2025GL119909 doi: 10.1029/2025gl119909

Parker, W. S. (2020). Model evaluation: An adequacy-for-purpose view. *Philosophy of Science*, *87*(3), 457–477. Retrieved from http://dx.doi.org/10.1086/708691 doi: 10.1086/708691

Quinting, J. F., & Reeder, M. J. (2017, October). Southeastern australian heat waves from a trajectory viewpoint. *Monthly Weather Review*, *145*(10), 4109–4125. Retrieved from http://dx.doi.org/10.1175/MWR-D-17-0165.1 doi: 10.1175/mwr-d-17-0165.1

Rigden, A. J., Mueller, N. D., Holbrook, N. M., Pillai, N., & Huybers, P. (2020, February). Combined influence of soil moisture and atmospheric evaporative demand is important for accurately predicting us maize yields. *Nature Food*, *1*(2), 127–133. Retrieved from http://dx.doi.org/10.1038/s43016-020-0028-7 doi: 10.1038/s43016-020-0028-7

Robine, J.-M., Cheung, S. L. K., Le Roy, S., Van Oyen, H., Griffiths, C., Michel, J.-P., & Herrmann, F. R. (2007, December). Death toll exceeded 70, 000 in europe during the summer of 2003. *Comptes Rendus. Biologies*, *331*(2), 171–178. Retrieved from http://dx.doi.org/10.1016/j.crvi.2007.12.001 doi: 10.1016/j.crvi.2007.12.001

Salley, S. W., Sleezer, R. O., Bergstrom, R. M., Martin, P. H., & Kelly, E. F. (2016). A long-term analysis of the historical dry boundary for the great plains of north america: Implications of climatic variability and climatic change on temporal and spatial patterns in soil moisture. *Geoderma*, *274*, 104–113. Retrieved from http://dx.doi.org/10.1016/j.geoderma.2016.03.020 doi: 10.1016/j.geoderma.2016.03.020

Santamouris, M., Cartalis, C., Synnefa, A., & Kolokotsa, D. (2015, July). On the impact of urban heat island and global warming on the power demand and electricity consumption of buildings—a review. *Energy and*

Buildings, *98*, 119–124. Retrieved from http://dx.doi.org/10.1016/j.enbuild.2014.09.052 doi: 10.1016/j.enbuild.2014.09.052

Santanello, J. A., Dirmeyer, P. A., Ferguson, C. R., Findell, K. L., Tawfik, A. B., Berg, A., ... Wulfmeyer, V. (2018, June). Land–atmosphere interactions: The loco perspective. *Bulletin of the American Meteorological Society*, *99*(6), 1253–1272. Retrieved from http://dx.doi.org/10.1175/BAMS-D-17-0001.1 doi: 10.1175/bams-d-17-0001.1

Schlenker, W., & Roberts, M. J. (2009, September). Nonlinear temperature effects indicate severe damages to u.s. crop yields under climate change. *Proceedings of the National Academy of Sciences*, *106*(37), 15594–15598. Retrieved from http://dx.doi.org/10.1073/pnas.0906865106 doi: 10.1073/pnas.0906865106

Schumacher, D. L., Keune, J., van Heerwaarden, C. C., Vilà-Guerau de Arellano, J., Teuling, A. J., & Miralles, D. G. (2019, August). Amplification of mega-heatwaves through heat torrents fuelled by upwind drought. *Nature Geoscience*, *12*(9), 712–717. Retrieved from http://dx.doi.org/10.1038/s41561-019-0431-6 doi: 10.1038/s41561-019-0431-6

Seneviratne, S. I., Corti, T., Davin, E. L., Hirschi, M., Jaeger, E. B., Lehner, I., ... Teuling, A. J. (2010, May). Investigating soil moisture–climate interactions in a changing climate: A review. *Earth-Science Reviews*, *99*(3–4), 125–161. Retrieved from http://dx.doi.org/10.1016/j.earscirev.2010.02.004 doi: 10.1016/j.earscirev.2010.02.004

Stull, R. B. (1988). *An introduction to boundary layer meteorology.* Springer Netherlands. doi: 10.1007/978-94-009-3027-8

Tennekes, H. (1973, May). A model for the dynamics of the inversion above a convective boundary layer. *Journal of the Atmospheric Sciences*, *30*(4), 558–567. Retrieved from http://dx.doi.org/10.1175/1520-0469(1973)030<0558:AMFTDO>2.0.CO;2 doi: 10.1175/1520-0469(1973)030⟨0558:amftdo⟩2.0.co;2

Teuling, A. J., Hirschi, M., Ohmura, A., Wild, M., Reichstein, M., Ciais, P., ... Seneviratne, S. I. (2009, January). A regional perspective on trends in continental evaporation. *Geophysical Research Letters*, *36*(2). Retrieved from http://dx.doi.org/10.1029/2008GL036584 doi: 10.1029/2008gl036584

Thornton, P., Nelson, G., Mayberry, D., & Herrero, M. (2021, August). Increases in extreme heat stress in domesticated livestock species during the twenty-first century. *Global Change Biology*, *27*(22), 5762–5772. Retrieved from http://dx.doi.org/10.1111/gcb.15825 doi: 10.1111/gcb.15825

Weaver, S. J., & Nigam, S. (2008, April). Variability of the great plains low-level jet: Large-scale circulation context and hydroclimate impacts. *Journal of Climate*, *21*(7), 1532–1551. Retrieved from http://dx.doi.org/10.1175/2007JCLI1586.1 doi: 10.1175/2007jcli1586.1

Xu, Y., He, Q., Lu, H., Yang, K., Entekhabi, D., & Short Gianotti, D. J. (2025, April). A global dataset of remote sensing-based soil critical point and permanent wilting point. *Scientific Data*, *12*(1). Retrieved from http://dx.doi.org/10.1038/s41597-025-05048-y doi: 10.1038/s41597-025-05048-y

Zeppetello, L. R. V., Battisti, D. S., & Baker, M. B. (2022, April). The physics of heat waves: What causes extremely high summertime temperatures? *Journal of Climate*, *35*(7), 2231–2251. Retrieved from http://dx.doi.org/10.1175/JCLI-D-21-0236.1 doi: 10.1175/jcli-d-21-0236.1

Zscheischler, J., Martius, O., Westra, S., Bevacqua, E., Raymond, C., Horton, R. M., ... Vignotto, E. (2020, June). A typology of compound weather and climate events. *Nature Reviews Earth & Environment*, *1*(7), 333–347. Retrieved from http://dx.doi.org/10.1038/s43017-020-0060-z doi: 10.1038/s43017-020-0060-z